Multielectron effects in capture of antiprotons and muons by helium and neon

James S. Cohen*
Theoretical Division, Los Alamos National Laboratory, Los Alamos, New Mexico 87545
(Received 9 December 1999; published 19 July 2000)

Antiproton ($\bar{p}$) and negative muon (μ^-) captures by helium and neon atoms are treated using the fermion-molecular-dynamics method, yielding capture cross sections, initial quantum numbers, and ejected-electron energies. The calculated angular-momentum distributions tend to pile up at $l=n-1$ and are not well fitted by the form $(2l+1)e^{\alpha l}$, which is often assumed in experimental analyses. The residual electrons are generally left in a ''shake-up'' state. When capture is accompanied by multiple ionization, the second and later electrons escape with increasing kinetic energies, a process that is not well described as quasiadiabatic. In a 50:50 mixture of helium and neon, the calculated Ne:He capture ratios are 3.36 for $\bar{p}$ and 3.69 for μ^-. The μ^- per-atom capture probability is almost independent of the neon fraction and is in overall agreement with several μ^- and π^- experiments; for $\bar{p}$ there is a rather strong dependence on neon fraction, but there are as yet no experiments. The possible experimental indication of a strong isotope effect on capture of π^- in mixtures of ^{3}He and ^{4}He is not supported by the present calculation.

PACS number(s): 36.10.−k, 34.10.+x, 25.43.+t, 03.65.Sq

I. INTRODUCTION

Atomic capture of heavy negative particles has been studied almost since the discovery of these particles.[1] Negative-particle collisions with atoms are fundamentally different from normal ion-atom collisions, as was first demonstrated experimentally by Barkas *et al.* [1]. The negative particle feels an increasingly attractive potential as it approaches the nucleus. One or more electrons can be ionized as the negative particle is captured. In this process, multiple electronic continua come into play and electron-electron as well as exotic particle-electron correlation may be important. Experiments have been conducted with all the noble-gas atoms, as well as with many simple and complex molecules [2].

The theory was pioneered by Fermi and Teller [3] using the Thomas-Fermi model for the target atom. Their model is fairly successful on the average, but its degenerate electron-gas treatment is not valid for light elements and does not allow for shell effects, first observed by Zinov *et al.* [4]. Most of the detailed theory has been done for the hydrogen *atom* [5,6], while capture by this simplest target is yet to be examined experimentally.[2] Several theoretical treatments of the hydrogen atom have shown that the capture energy primarily goes to target ionization with the ionized electron carrying off little kinetic energy, as predicted by the adiabatic-ionization model [8]. Capture by multielectron atomic targets involves additional questions: (i) how many electrons are ionized, (ii) is the target atom left in its ground electronic state immediately after capture, and (iii) are the electrons ionized with very low kinetic energy? The analog to the adiabatic-ionization model would suggest the answer to (i) is the minimum number consistent with positive answers to (ii) and (iii).

It can be inferred from experimental observations of relative capture probabilities that additional electrons tend to increase the capture probability, though not monotonically; simple Z scaling [3] is clearly inadequate. The opposite supposition, that the capture cross section depends mainly on the target ionization potential, as suggested by capture occurring at low collision energies, is also clearly inconsistent with the data. Semiempirical formulas [9–11], motivated by these and other considerations, have been fairly successful in fitting the observed capture probabilities, but leave many basic questions, like those above, unanswered. In the present paper, we report calculations on helium and neon, the simplest atoms for which experiments have been performed [12–15].

Answering these questions requires a theoretical method capable of treating all electron dynamics, including multiple ionization and correlation. Previous work showed that muon-electron correlation is essential in capture by the hydrogen atom [16]. These demands exceed the capability of any existing fully quantum-mechanical method, but are treatable by the quasiclassical method known as fermion molecular dynamics (FMD) [17]. The FMD method uses pseudopotentials to approximate quantum-mechanical behavior and formulate the problem within Hamilton's equations of motion. It accounts for the three-dimensional, correlated motion of all electrons.

A recent experiment on μ^- capture by neon [18] has provided unprecedented information on the initial capture. Comparison with the present calculations yields new understanding of the mixed electronic-muonic state.

II. METHOD

A. Fermion molecular dynamics

The FMD method has previously been described in detail [17]. It utilizes the Kirschbaum-Wilets (KW) ansatz for the

*Electronic address: cohen@lanl.gov

[1]Muon μ^- of mass $206.77m_e$ (in 1937), pion π^- of mass $273.14m_e$ (in 1947), kaon K^- of mass $966.04m_e$ (in 1947), and antiproton $\bar{p}$ of mass $1836.15m_e$ (in 1955).

[2]The ASACUSA collaboration [7] is preparing an experiment on $\bar{p}$ capture by the hydrogen atom using the new antiproton decelerator (AD) at CERN.

TABLE I. Optimized FMD parameters. In all cases, $\alpha_H = 2.0$ and $\alpha_P = 1.0$.

	FMD parameters		Associated energies	
	ξ_H	ξ_P	IP_1 (a.u.)	E_{tot} (a.u.)
H	0.8946		0.4998	−0.4998
He	0.9343		0.9737	−2.807
Li	0.9116	4.066	0.1981	−7.478
Be	0.9014	4.924	0.3425	−14.67
B	0.9369	2.378	0.3050	−24.66
C	0.9424	2.332	0.4138	−37.86
N	1.0167	1.840	0.5340	−54.61
O	0.9881	1.996	0.5006	−75.11
F	1.1244	1.464	0.6402	−99.81
Ne	1.1311	1.511	0.7924	−129.1

[a]For He, the FMD parameters were chosen to minimize a weighted error in IP_1 and E_{tot}; the exact values are 0.9037 and −2.904, respectively.

atomic structure [19]; pseudopotentials V_H and V_P, which constrain the quasiclassical dynamics to satisfy the Heisenberg uncertainty and Pauli exclusion principles, respectively, stabilize the quasiclassical multielectron atom and provide a shell structure [20]. Similar terms are included for the exotic atom structure, but have little effect since it is formed in a highly excited state, which behaves nearly classically according to the correspondence principle.

The FMD effective Hamiltonian for the system is written

$$H_{\mathrm{FMD}} = H_0 + V_H + V_P, \tag{1}$$

where H_0 is the usual Hamiltonian of the system containing the kinetic energies of all particles and Coulomb potentials for all pairs of particles. The extra terms are

$$V_H = \sum_{i=1}^{N_e} f(r_{ni}, p_{ni}; \xi_H, \alpha_H) + f(r_{nx}, p_{nx}; \xi_H, \alpha_H) \tag{2}$$

and

$$V_P = \sum_{i=1}^{N_e} \sum_{j=i+1}^{N_e} f(r_{ij}, p_{ij}; \xi_P, \alpha_P)\, \delta_{s_i, s_j}, \tag{3}$$

where r_{ni} is the distance of electron i from the nucleus n, r_{nx} is the distance of the exotic particle x from the nucleus n, r_{ij} is the distance between electrons i and j, and s_i is the spin of electron i.

As usual in the FMD method, the constraining potentials are chosen to be of the form [19]

$$f(r_{\lambda\nu}, p_{\lambda\nu}; \xi, \alpha) = \frac{(\xi\hbar)^2}{4\alpha r_{\lambda\nu}^2 \mu_{\lambda\nu}} \exp\left\{ \alpha \left[1 - \left(\frac{r_{\lambda\nu} p_{\lambda\nu}}{\xi\hbar} \right)^4 \right] \right\}, \tag{4}$$

where subscripts λ and ν designate pairs of particles with reduced mass $\mu_{\lambda\nu}$. The parameter ξ reflects the size of the core (Heisenberg or Pauli) while α is a hardness parameter. The only way in which we deviate from the original prescription of KW is to use values of ξ_H and ξ_P optimized for the target atom, rather than the universal values, and softer values of α_H and α_P, as later recommended by Beck and Wilets [21]. The modification of the hardness parameters α_H and α_P is not as important for the low-energy collisions under present consideration as it was for the stopping powers calculated by Beck and Wilets, but we use the same values $\alpha_H = 2.0$ and $\alpha_P = 1.0$.

The values of ξ_H and ξ_P were chosen to match the first ionization potential and total binding energy of the target atom, since the first ionization potential is most important for the capture dynamics and the higher ionization potentials on the average will be correct. This procedure is exact for all atoms except He, for which the parameter ξ_P has no effect since its two electrons have antiparallel spins. (α_H and α_P are not useful variables for this procedure.) The parameters obtained for the atoms H through Ne are given in Table I.

Beyond the Monte Carlo statistical errors, the main uncertainties in these calculations come from the use of quasiclassical dynamics and the approximate target shell structure, as discussed above. Although there are no comparable calculations of capture of exotic particles by multielectron targets, some indications of the accuracy of the FMD method can be gained from comparisons of FMD calculations of capture by the hydrogen atom with accurate quantum-mechanical calculations [6] and comparisons of FMD calculations of ionization and electron transfer in ion-atom collisions with experiments [22]. The comparisons, in Secs. IV and V, of some calculated features with experiments, will also help gauge the accuracy.

B. Pseudoquantum numbers

In order to model the cascade, the distributions of n and l quantum numbers of the capture orbital are needed as well as the total capture cross section. Because the n values are large ($\gtrsim \sqrt{m_x/m_e}$) the quasiclassical assignment by binning is quite satisfactory. However, there is still uncertainty that arises from approximating the structure actually calculated with single-particle (hydrogenlike) quantum numbers when in fact there may be residual electrons present. This compli-

cation does not directly affect the angular momentum l of the exotic particle with respect to the nucleus, but does affect its association with a given n, which is important in determining the probabilities of subsequent radiative and Auger cascade transitions [23,24]. The direct transfer of angular momentum between the exotic particle and the electrons is relatively small. We have taken two different approaches to this problem: (1) using the full nuclear charge ignoring the electrons and (2) using an effective nuclear charge to approximate electron screening, as follows.

1. Two-body approach

Two-particle binding is calculated simply as

$$E_2 = -\frac{Z}{r} + \frac{p_{\rm rel}^2}{2\mu}, \tag{5}$$

where r and $p_{\rm rel}$ are the distance and momentum of the captured exotic particle relative to the nucleus of charge Z and μ is its reduced mass. Then this quantum number, which we denote n_2, is given by

$$n_2 = \left(\frac{-\mu Z^2}{2E_2} \right)^{1/2} \tag{6}$$

(actually the nearest integer). One advantage of this approach is that the inequality $l \leqslant n_2$ (nonintegerized values) rigorously holds (see the Appendix). With the identification $[l] \rightarrow l$ and $[n_2+0.5] \rightarrow n$, the quantum-mechanical relation $l \leqslant n-1$ is essentially satisfied for large n ($[x]$ designates the greatest integer less than or equal to x).

2. Screening approach

The effective n, taking screening into account, is not unique. We calculate the energy of the total system $E_{\rm tot}$ (including even apparently free electrons) and the energy of the system with the exotic particle removed E_{-x}; the difference yields the effective binding energy

$$E_{\rm eff} = E_{\rm tot} - E_{-x}. \tag{7}$$

The effective nuclear charge $Z_{\rm eff}$ is then taken to be the charge that would exert the actual *central* component of force on the exotic particle if there were no electrons; i.e.,

$$\frac{-Z_{\rm eff}}{|\mathbf{r}_x - \mathbf{r}_n|^2} = -\frac{(\mathbf{r}_x - \mathbf{r}_n)}{|\mathbf{r}_x - \mathbf{r}_n|} \cdot \boldsymbol{\nabla}_{\mathbf{r}_x} H. \tag{8}$$

Then

$$n_{\rm eff} = \left(\frac{-\mu Z_{\rm eff}^2}{2E_{\rm eff}} \right)^{1/2}. \tag{9}$$

Due to the electrons, the effective potential is neither Coulomb nor central, and the relation $l \leqslant n_{\rm eff}$ does not necessarily apply. Since circular orbitals ($l = n-1$) pose bottlenecks for the subsequent cascade and are thus particularly important, method (2) may be seriously deficient.

III. CAPTURE OF $\bar{p}$ AND μ^- BY HELIUM

The simplest physical system for which exotic-particle capture experiments have been performed is the helium atom. These experiments include capture ratios for muons [12,13] and pions [14,15] in mixtures of helium with other gases, the x-ray cascade of muonic [25–31], pionic [25,27,32,33], and antiprotonic [34–36] helium, and, most recently, spectroscopy of the metastable electron-antiproton system $\alpha\bar{p}e^-$ [37–40]. Capture of exotic particles by helium has previously been treated theoretically by a variety of approximations, including plane-wave Born [41] ($\mu^-, \pi^-, K^-, \bar{p}$), Coulomb-Born [42] ($\mu^-$), optical potential with Hartree-Fock wave functions [43] (μ^-), diabatic states [44] ($\mu^-, \pi^-, K^-, \bar{p}$), coupled-channel semiclassical [45] ($\mu^-, \pi^-, K^-, \bar{p}$), nonadiabatic black body [46] ($\mu^-, \bar{p}$), and FMD [47] ($\bar{p}$). Apart from the first two perturbative methods, all these calculations agree that the exotic particles are captured only after being slowed to kinetic energies comparable to the first ionization potential of the target helium atom.

The previous FMD calculation on $\bar{p}$ capture by He was mainly concerned with characterizing long-lived states of the $\alpha\bar{p}e^-$ system [47]. That work found that about 22% of the antiprotons captured by He survived in the three-body system beyond times of 10^5 a.u. (2.4 ps). Here we take a similar approach in following the dynamics long enough that prompt ionization of the second electron has an opportunity to occur, which usually takes $\lesssim 0.1$ ps. Characterization of the states after prompt ionization is most relevant to experiments. In essential agreement with Beck *et al.* [47], we find that 20% of the $\alpha\bar{p}e^-$ escape prompt ionization and survive beyond 1 ps. In similar calculations of μ^- capture by helium, we find a somewhat smaller fraction 14% surviving beyond 1 ps. At longer times the calculated decay is much slower. However, characterization of the behavior at the experimental time of $\sim \mu$s by the present approach is impractical because of the extreme number of integration steps that would be required, and in any case would be of dubious validity with the quasiclassical description.

The distributions of principal quantum numbers n, determined at ~ 0.3 ps, are shown in Figs. 1(a) and 1(b) for $\bar{p}$ and μ^- capture, respectively, by He. The distributions peak at $n=34$ for $\bar{p}\alpha$ and $n=12$ for $\mu^-\alpha$. The shoulder, visible in both cases on the high-n side, corresponds to systems still retaining one electron, generally with the electron having large l as well as large n. These distributions have been integrated over capture energy, weighted by the capture fraction $\sigma_{\rm capt}(E)/\sigma_{\rm tot}(E)$, as is appropriate for situations in which the exotic particle is slowed down and captured in the target medium. Figure 2 shows the distribution for $\bar{p}$ capture at a particular energy ($E_{\rm c.m.}=0.4$ a.u.). This distribution clearly reveals the separation of the $\bar{p}\alpha$ states at low n and $\bar{p}\alpha e^-$ states at high n. The $\bar{p}\alpha e^-$ states have small values of $n-l$ and decay on a time scale at least an order of magnitude slower.

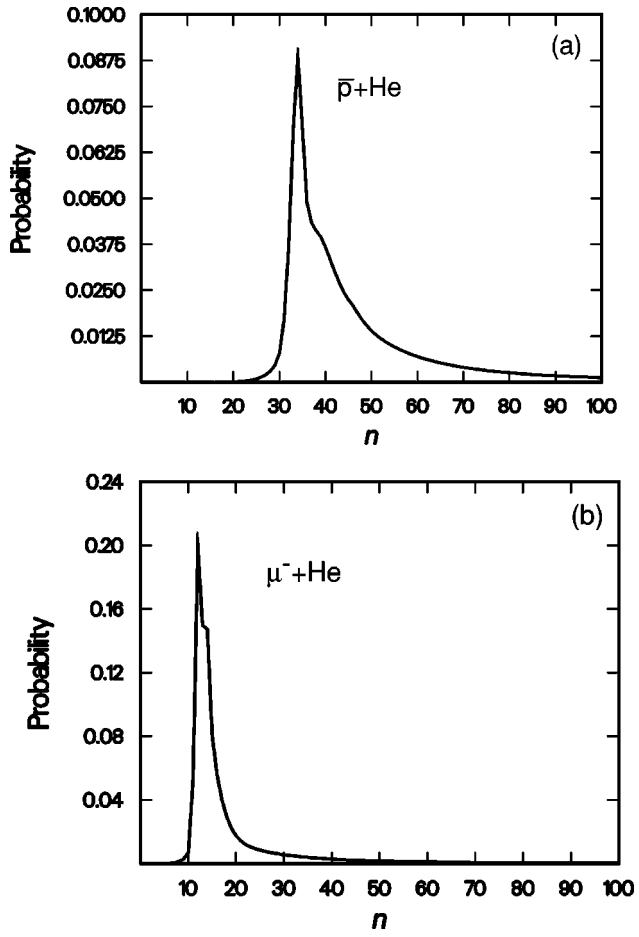

FIG. 1. Principal quantum number n distributions (integrated over capture collision energies) for (a) $\bar{p}$ and (b) μ^- capture by helium. These distributions were obtained at a time of ~ 0.3 ps after the arrival of the projectile at the target. At the peaks both electrons are ionized, but in the region of the shoulder and higher some atoms retain an electron.

The most useful l distributions are for given n since it is $n-l$ that tends to be most important in determining cascade steps. Frequently this distribution has been approximated by the form $(2l+1)e^{\alpha l}$ for $0 \leqslant l < n$, where $\alpha = 0$ corresponds to a statistical distribution, $\alpha > 0$ to overpopulation of large l, and $\alpha < 0$ to underpopulation of large l. This characterization is most important at $n \approx n_0 = \sqrt{m_x/m_e}$; for very large n ($\gg n_0$), the population will cut off at $l < n$ since particles with very large l do not penetrate to distances where the electron density and capture probability are large. In Fig. 3 the l distributions for $\bar{p}\alpha(n=34)$ and $\mu^-\alpha(n=12)$, integrated over capture energy, are shown. For $\bar{p}\alpha$, the l distribution is fairly statistical at low-to-moderate values of l and peaks strongly at $l = n-1$, with a valley in between. A similar behavior is seen for $\mu^-\alpha$, with the peak at $l = n-1$ not quite so pronounced. Obviously this sort of distribution cannot be accurately represented by the form $(2l+1)e^{\alpha l}$.

The capture and total ionization cross sections for antiproton and muon capture by helium are enumerated in Table II and shown in Figs. 4(a) and 4(b), respectively. As required for conservation of energy, the capture and total ionization

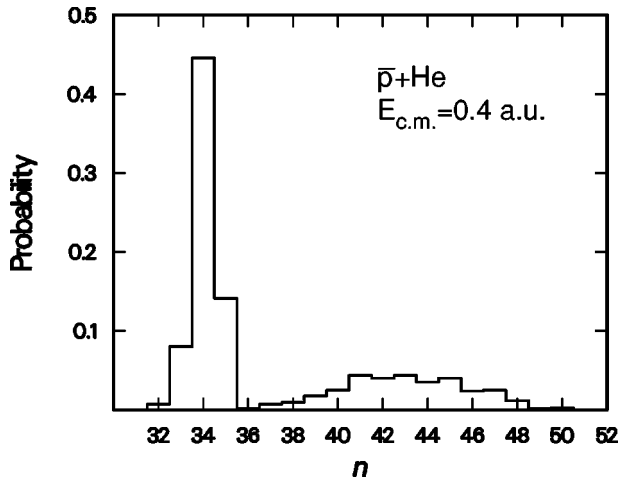

FIG. 2. Principal quantum number n distribution for $\bar{p}$ captured by helium in a collision at center-of-mass energy 0.4 a.u. The population in the second peak at higher n retains an electron in a relatively long-lived high-l state.

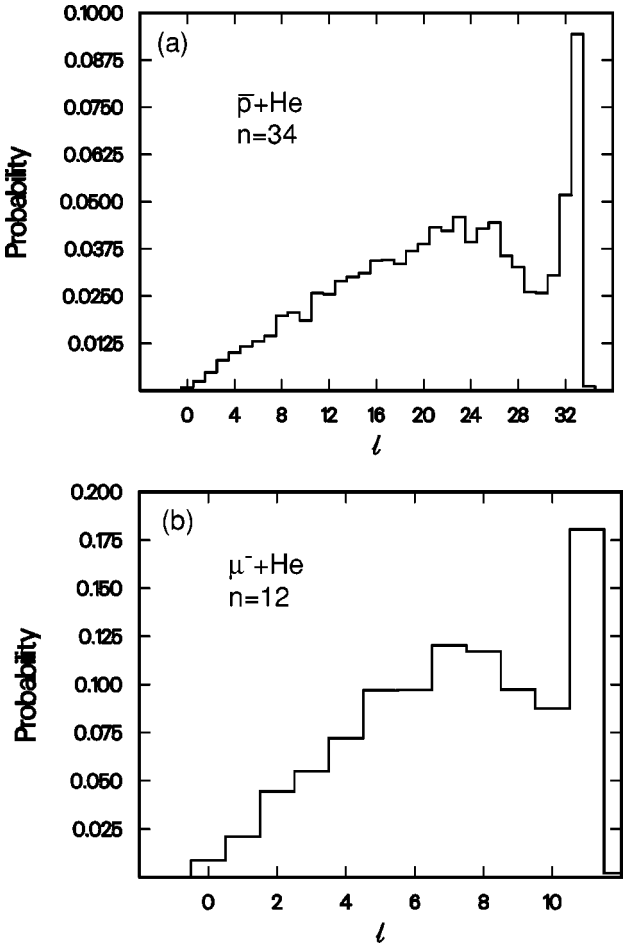

FIG. 3. Angular-momentum l distributions for (a) $\bar{p}$ captured by helium in $n=34$ and (b) μ^- captured by helium in $n=12$ (the most probable n in Fig. 1). (*Note:* In this histogram the statistical error is $\sim 15\%$; i.e., fine-scale roughness in this and other histograms is not significant.)

TABLE II. Capture and total ionization cross sections for (a) $\bar{p}$+He and (b) μ^-+He.

$E_{c.m.}$ (a.u.) [a]	σ_{capt} (units of a_0^2) [a]	σ_{tot} (units of a_0^2)	$E_{c.m.}$ (a.u.) [a]	σ_{capt} (units of a_0^2) [a]	σ_{tot} (units of a_0^2)
	(a) $\bar{p}$+He			(b) μ^-+He	
0.01	77.76±1.13	77.76±1.13	0.01	72.31±1.17	72.31±1.17
0.10	18.20±0.28	18.20±0.28	0.10	18.98±0.28	18.98±0.28
0.20	9.55±0.14	9.55±0.14	0.20	10.42±0.13	10.42±0.13
0.30	6.90±0.09	6.90±0.09	0.30	7.59±0.12	7.60±0.12
0.40	5.34±0.06	5.34±0.06	0.40	6.05±0.08	6.06±0.08
0.50	4.56±0.07	4.56±0.07	0.50	5.13±0.07	5.16±0.07
0.60	3.94±0.06	3.94±0.06	0.60	4.54±0.07	4.59±0.07
0.70	3.54±0.05	3.54±0.05	0.70	4.12±0.07	4.17±0.07
0.80	3.27±0.04	3.27±0.04	0.80	3.80±0.06	3.89±0.06
0.90	3.05±0.05	3.07±0.05	0.90	3.59±0.06	3.69±0.06
1.00	2.91±0.05	2.95±0.05	1.00	3.41±0.05	3.57±0.06
1.10	1.76±0.07	2.80±0.05	1.10	2.91±0.06	3.56±0.06
1.20	0.95±0.06	2.70±0.05	1.20	2.02±0.07	3.35±0.06
1.50	0.38±0.05	2.41±0.06	1.50	1.02±0.07	3.21±0.07
2.00	0.10±0.03	2.17±0.06	2.00	0.59±0.05	3.19±0.08
2.50	0.01±0.01	2.03±0.07	2.50	0.33±0.04	3.20±0.08
3.00		1.90±0.05	3.00	0.09±0.02	3.19±0.07
4.00		1.82±0.05	4.00		3.30±0.07
6.00		1.84±0.05	6.00		3.40±0.07
8.00		1.91±0.05	8.00		3.48±0.07
10.00		2.06±0.06	10.00		3.47±0.07
12.00		2.28±0.06	12.00		3.59±0.07
15.00		2.36±0.06	15.00		3.55±0.07
18.00		2.59±0.07	18.00		3.69±0.07
21.00		2.60±0.06	21.00		3.63±0.07
25.00		2.74±0.07	25.00		3.74±0.07
30.00		2.95±0.07	30.00		3.89±0.07

[a] 1 a.u.=27.21 eV; $1a_0^2=0.280\times10^{-16}$ cm^2.

cross sections coincide at collision energies below the first ionization potential of the target. Like the hydrogen atom target, it is still generally true that capture by the helium atom occurs with ionization of a single electron. The kinetic-energy distributions of the first ejected electron are shown in Figs. 5(a) and 5(b) for $\bar{p}$ and μ^- capture, respectively, by helium.

Strictly speaking, adiabatic ionization cannot occur for the He target since the adiabatic correlation is to H^-, which is bound. In a quasiadiabatic description, the first electron ejected has near-zero kinetic energy. It can be seen by comparing Figs. 5(a) and 5(b) that the heavier $\bar{p}$ behaves more adiabatically than does the lighter μ^-. The average electron energy for the former is 0.10 a.u., for the latter 0.15 a.u. This can be compared to 0.05 a.u. and 0.09 a.u. for $\bar{p}$+H and μ^-+H, respectively. Though the behavior with helium is less adiabatic than with the hydrogen atom, the simple quasiadiabatic picture still has some qualitative validity. The capture cross section falls off fairly rapidly at collision energies above the first ionization potential. This finding is in agreement with earlier diabatic-state (DS) calculations of exotic helium formation [44]; the DS treatment yields cross sections, which elude the purely adiabatic treatment.

In most cases it is the ionization of the first electron that effects capture by helium. The second electron then usually follows by an internal Auger process in which the captured $\bar{p}$ deexcites. However, the two physical processes are similar and there is sometimes not a sharp separation. In fact, careful comparison of Fig. 4(a) with Fig. 5(a) and Fig. 4(b) with Fig. 5(b) reveals that the capture cross section is still significant at energies exceeding the target first ionization potential by more than the maximum kinetic energy of the first ejected electron. This is evidence of participation of the second electron in the *initial* capture. In the case of $\bar{p}$ it appears that the second electron is left excited but not ionized; for μ^- the second electron may sometimes be ionized since the capture cross section extends to energies exceeding the total binding energy of the helium atom (2.81 a.u. in our FMD description).

IV. CAPTURE OF $\bar{p}$ AND μ^- BY NEON

The cross sections for $\bar{p}$ and μ^- reactions with neon are enumerated in Table III and shown in Fig. 4 along with the

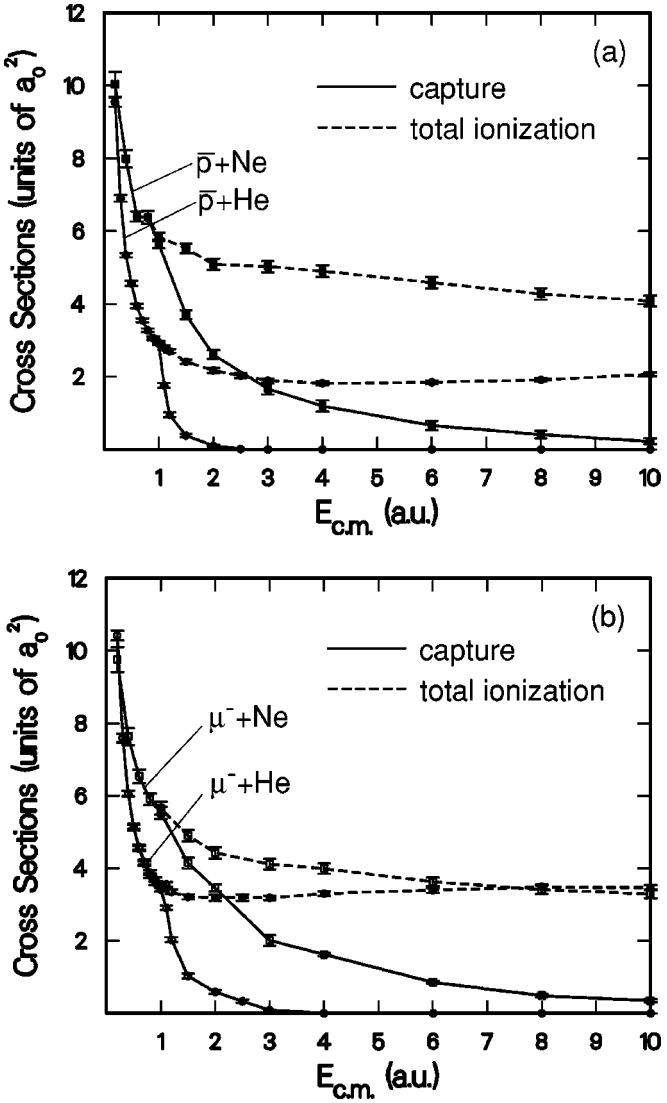

FIG. 4. Capture (solid curves) and total-ionization (dashed curves) cross sections for (a) $\bar{p}$ collisions with helium (closed-circular points) and neon (closed-square points) and (b) μ^- collisions with helium (open-circular points) and neon (open-square points). The error bars indicate the Monte Carlo statistics.

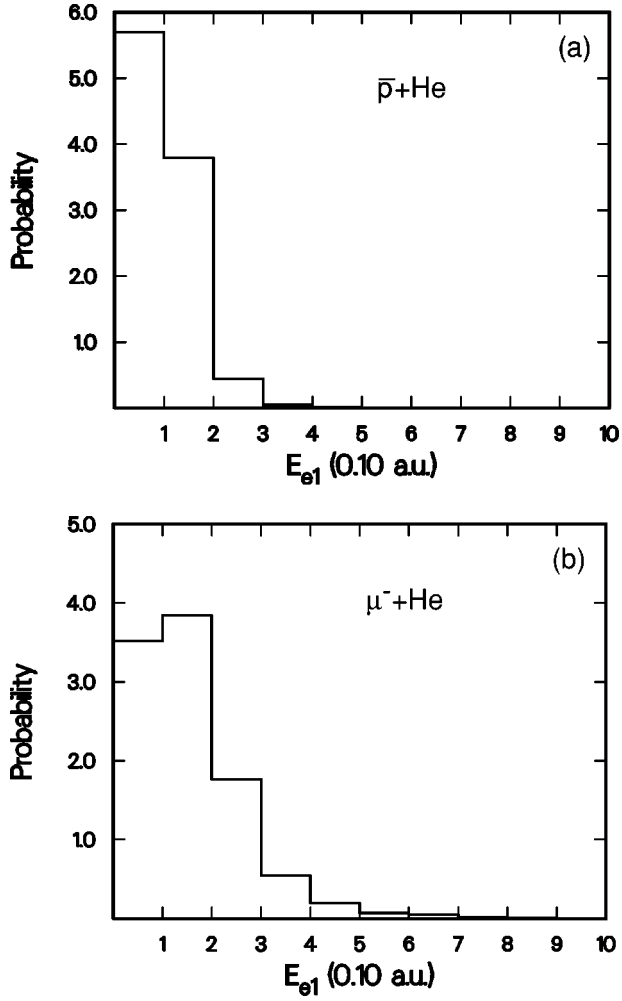

FIG. 5. Distributions of the kinetic energies of the first electron ejected in collisions where (a) $\bar{p}$ and (b) μ^- are captured by helium.

helium cross sections. The capture cross sections for neon reach considerably higher collision energies than for helium, still significant at ~ 10 a.u. While Figs. 6(a) and 6(b) show that the first ejected electron carries off about twice as much kinetic energy (average 0.21 a.u. for $\bar{p}+\mathrm{Ne}$ and 0.34 a.u. for $\mu^-+\mathrm{Ne}$) than in the case of helium targets, it is still evident that more than one electron must be ionized to effect capture at such high collision energies. Subsequent electrons have higher ionization potentials, and the calculations show that they escape with increasingly higher kinetic energies. The kinetic-energy distributions for the second ejected electron are shown in Figs. 7(a) and 7(b); on the average, the energies of the second electron are about twice as large as for the first electron. Nonetheless, even more electrons must be ionized for capture to occur at collision energies as high as 10 a.u.

The calculations of capture by neon were carried out with a somewhat different strategy than those for helium. Though the captures at high energies require ionization of multiple electrons, we certainly want to characterize the state before all ten electrons are ionized. Since the time-dependent transfer of energy from the heavy negative particle to the electrons can be nonmonotonic, the ''instant'' of capture is not a well-defined quantity, nor is the initial n quantum number. The chosen strategy, consistent with a typical experimental analysis [18], is to follow each trajectory until some more-or-less arbitrary n value is reached. The values chosen were 45 for $\bar{p}+\mathrm{Ne}$ and 16 for $\mu^-+\mathrm{Ne}$.

The number of electrons remaining at this point is important to the subsequent cascade, which initially proceeds by Auger conversion of electrons as the exotic particle deexcites to lower orbitals. Actually the ion is left in a shake-up state and some electrons will simultaneously be removed by purely electron-electron interactions. We attempt to deal with this situation by utilizing two limiting measures of the number of bound electrons: (i) counting all remaining electrons, no matter how weakly bound and (ii) counting only the electrons that would remain bound if electronic Auger processes proceeded to completion while the exotic particle re-

TABLE III. Capture and total ionization cross sections for (a) $\bar{p}$+Ne and (b) μ^-+Ne.

$E_{\text{c.m.}}$ (a.u.)	σ_{capt} (units of a_0^2)	σ_{tot} (units of a_0^2)
	(a) $\bar{p}$+Ne	
0.01	32.23±1.98	24.32±1.98
0.10	13.82±0.41	13.82±0.41
0.20	10.04±0.35	10.04±0.35
0.40	7.99±0.24	7.99±0.24
0.60	6.41±0.14	6.41±0.14
0.80	6.38±0.17	6.38±0.17
1.00	5.66±0.13	5.84±0.11
1.50	3.71±0.12	5.53±0.13
2.00	2.61±0.12	5.09±0.15
3.00	1.66±0.16	5.03±0.16
4.00	1.19±0.15	4.90±0.16
6.00	0.66±0.13	4.59±0.16
8.00	0.41±0.11	4.27±0.16
10.00	0.22±0.08	4.08±0.15
12.00	0.03±0.03	4.05±0.15
15.00		4.04±0.17
18.00		3.92±0.17
21.00		3.80±0.15
25.00		3.70±0.15
30.00		3.72±0.16
	(b) μ^-+Ne	
0.01	36.19±2.20	24.88±2.39
0.10	12.82±0.51	12.44±0.50
0.20	9.75±0.35	9.75±0.35
0.40	7.63±0.23	7.63±0.23
0.60	6.53±0.19	6.53±0.19
0.80	5.91±0.16	5.91±0.16
1.00	5.53±0.17	5.66±0.17
1.50	4.15±0.15	4.90±0.16
2.00	3.46±0.10	4.43±0.16
3.00	2.01±0.15	4.12±0.15
4.00	1.63±0.05	3.99±0.15
6.00	0.86±0.03	3.63±0.13
8.00	0.49±0.04	3.41±0.12
10.00	0.35±0.04	3.29±0.12
12.00	0.22±0.03	3.20±0.12
15.00	0.10±0.02	2.92±0.10
18.00	0.03±0.01	2.88±0.10
21.00	0.03±0.01	2.83±0.10
25.00	0.01±0.01	2.62±0.10
30.00		2.52±0.10

mained frozen in its initial state ($n=45$ for $\bar{p}$Ne and $n=16$ for μ^-Ne). The latter measure is approximated by comparing the energy of the electronic system with the *ground-state* energy of the ion having just lower energy. The minimum number of residual electrons is obtained by supposing that each ejected electron carries off negligible kinetic energy.

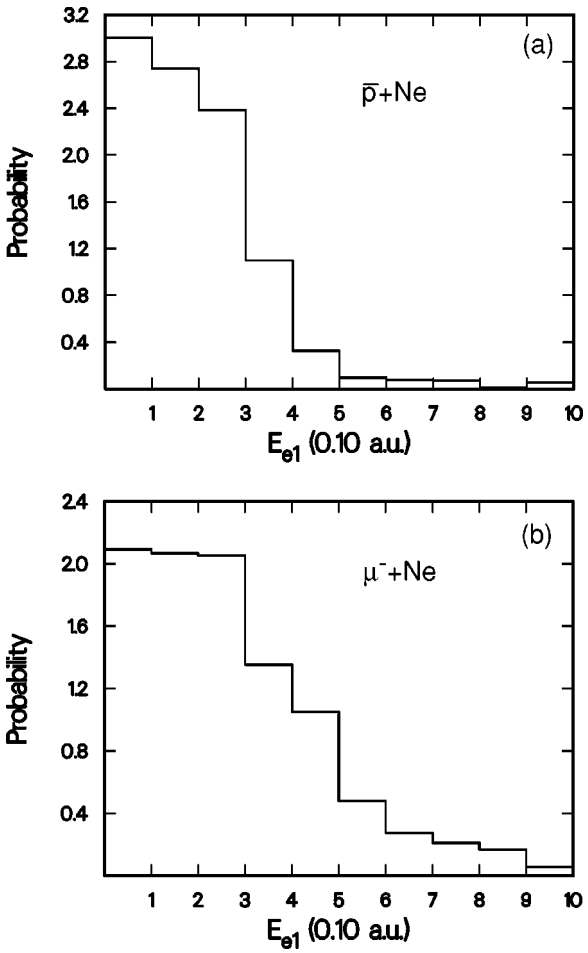

FIG. 6. Distributions of the kinetic energies of the first electron ejected in collisions where (a) $\bar{p}$ and (b) μ^- are captured by neon.

The *effective* number of electrons should lie in between these two measures.

The number of bound electrons, determined by these two measures, accompanying $\bar{p}$Ne($n=45$) and μ^-Ne($n=16$) are shown in Figs. 8(a) and 8(b), respectively. The experimental analysis of Kirch *et al.* [18] found a best fit for μ^-Ne at $n=16$ with $n_e=4.7^{+0.8}_{-0.3}$. They interpreted a fractional value of n_e as a mixture of the next lower and next higher integer charges, though higher and lower charge states cannot really be precluded. This experimental distribution agrees well with the measure (ii) in Fig. 8(b). This finding is consistent with both the fast reaction times for the light electrons and the weak interaction between the muon and very diffuse electrons.

The situations of μ^-Ne($n=16$) and $\bar{p}$Ne($n=45$) appear to be similar. This is as expected since the binding energies $-m_x/2n_x^2$ of these two states are about equal [actually the mass ratio would imply $n=46.7$ for the $\bar{p}$Ne with the same energy as $n=16$ of μ^-Ne, which is consistent with n_e in Fig. 8(a) being a bit smaller than in Fig. 8(b)].

We now consider the angular-momentum distributions. The analysis was done with both the n_2 of Eq. (6) and n_{eff} of Eq. (9). The description with n_2 was found to converge somewhat more rapidly and to have other apparent advan-

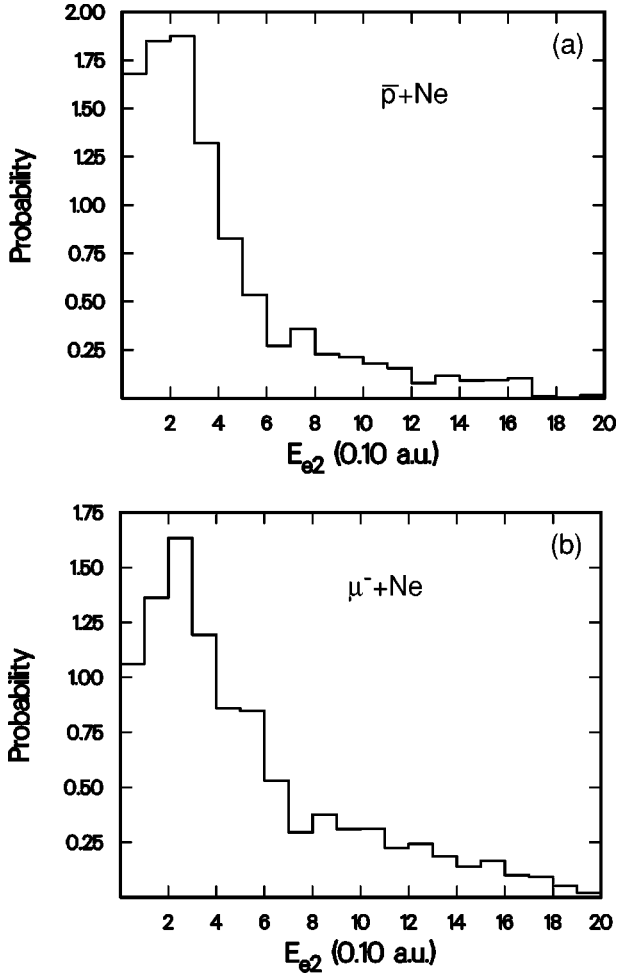

FIG. 7. Distributions of the kinetic energies of the second electron ejected in collisions where (a) $\bar{p}$ and (b) μ^- are captured by neon.

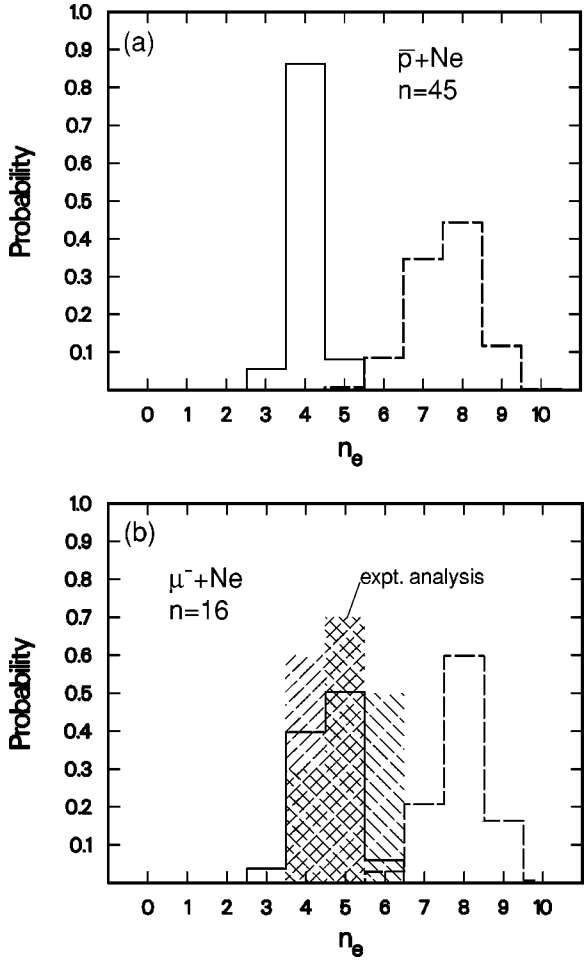

FIG. 8. Number of residual bound electrons when (a) $\bar{p}$Ne reaches $n=45$ and (b) μ^-Ne reaches $n=16$. The dashed histogram includes weakly bound electrons; the solid histogram counts only electrons that would still be bound after electron-electron Auger relaxation. In (b), the hatched area shows the results of the experimental analysis (Ref. [18]), $n_e=4.7^{+0.8}_{-0.3}$, with the *assumption* that only the next-lower and next-higher charge states occur (the cross-hatched area corresponds to $n_e=4.7$).

tages, but both will be presented. The results for $\bar{p}$Ne($n_2=45$) and μ^-Ne($n_2=16$) are shown in Figs. 9(a) and 9(b), respectively. They display a flat-to-statistical shape for low-to-moderate l and a strong peak at $l=n-1$. This pileup may be attributed in part to the initial steps of the cascade. To the extent it can be ascertained, the initial capture often occurs in still higher n. In some cases this is significantly higher than the l values where capture occurs, those being limited to impact parameters about equal to the size of the target atom. However, for purpose of experimental analysis, it is more relevant to initialize the cascade at the moderate values.

Such an experimental analysis has been done for μ^- capture by neon [18]. A form $P(l)\propto(2l+1)e^{\alpha l}$ was *assumed* and a best fit was obtained with $\alpha=0.090^{+0.035}_{-0.015}$, as shown in Fig. 9(b). This curve is like the theoretical distribution in enhancing the largest allowed l, but the form is clearly incapable of faithfully representing the theoretical populations. It should be noted that the simple exponential factor has no real theoretical basis. This form would do an even poorer job of fitting the theoretical angular-momentum distribution shown in Fig. 9(a) for $\bar{p}$Ne.

The theoretical angular-momentum distributions have also been calculated taking electron screening into account using Eqs. (7)–(9). The effective nuclear charge, which would yield the same force toward the nucleus, is calculated by Eq. (8) and shown in Figs. 10(a) and 10(b) for the capture orbitals of $\bar{p}$Ne and μ^-Ne, respectively. The effective nuclear charges felt by $\bar{p}$ in $n_{\rm eff}=45$ and μ^- in $n_{\rm eff}=16$, determined by Eq. (9), are similar; somewhat less than half of the captured exotic particles feel the full nuclear charge and a few are subject to an effective charge as small as 4 at this point. The corresponding angular-momentum distributions are shown in Fig. 11. As in Fig. 9, the distributions strongly peak at the largest l populated. However, this maximum l value is here less than $n_{\rm eff}-1$; evidently the centrifugal barrier is also distorted by the electrons. This shift of the angular-momentum end point demonstrates the inadequacy of the hydrogenic orbital treatment. But if such a model must be used, it could cause a serious error to really take $l_{\rm max}<n-1$. Since present practical treatments use the effective

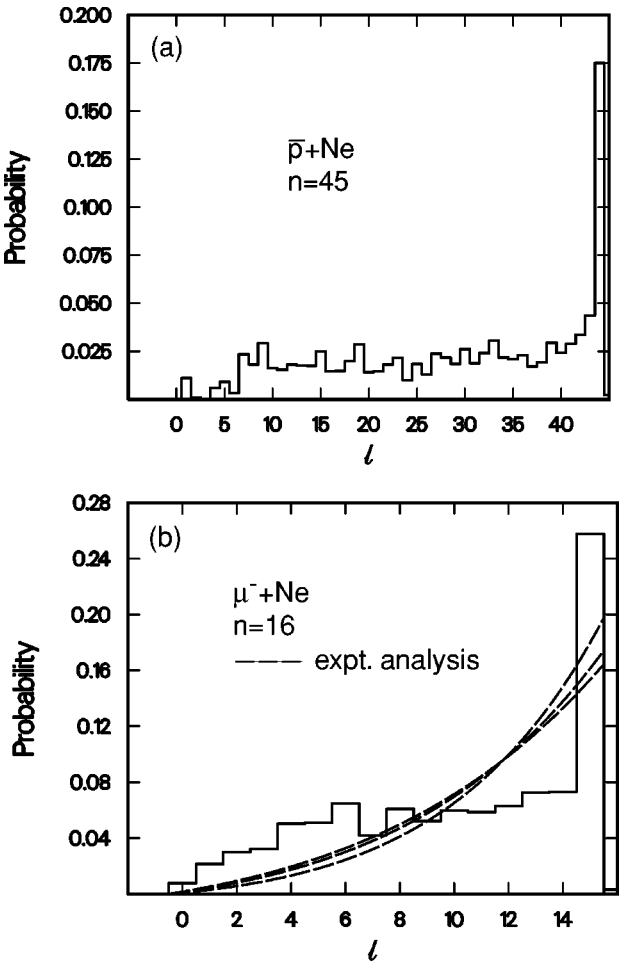

FIG. 9. Angular-momentum l distributions for (a) $\bar{p}$ captured by neon in $n=45$ and (b) μ^- captured by neon in $n=16$. This analysis was done with the n quantum number defined by Eq. (6). The dashed curves in (b) are the experimental fits (Ref. [18]) obtained assuming the form $(2l+1)e^{\alpha l}$ with $\alpha=0.090$ (central value) and 0.075 and 0.125 (error limits).

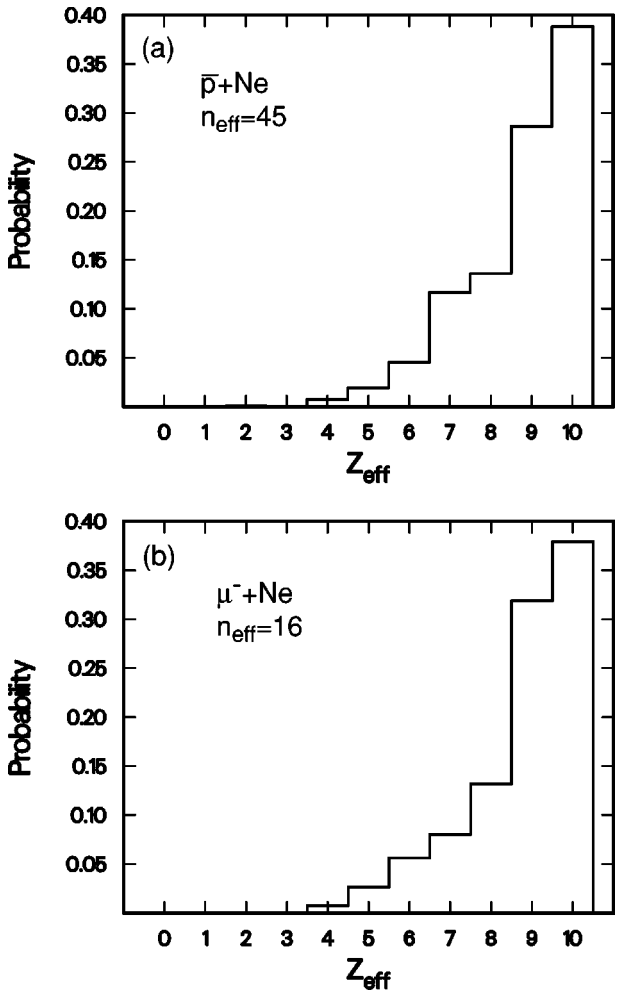

FIG. 10. Effective nuclear charges felt by the (a) $\bar{p}$ and (b) μ^- initially captured by neon.

single-particle model, it is probably more appropriate to use the distributions shown in Fig. 9.

V. CAPTURE IN MIXTURES OF HELIUM AND NEON

In this section we consider the capture of $\bar{p}$ and μ^- in a *thick* target of uniformly mixed helium and neon (''thick'' here means that both the slowing down and capture of an initially energetic $\bar{p}$ or μ^- occur within the medium). Capture of a monoenergetic beam in a *thin* target would depend only on the capture cross sections at that energy, but capture in a thick target depends on the slowing down history as well as the energy-dependent capture cross sections. Rigorous calculation would require solution of an integral equation for the arrival function (spectral flux density) starting with exotic particles at energies much higher than where capture occurs [48]. We have not calculated the slowing-down cross sections at such energies; however, other work suggests that the arrival function for heavy negative particles tends to be rather flat [49]. This is because slowing down occurs by much the same mechanism as capture, namely ionization, and thus the energy steps in the slowing down are similar to the energies where capture occurs. A flat arrival function justifies calculation of capture distributions by quadratures over the capture cross sections; e.g., in the case of principal quantum number n,

$$P(n)\approx N\int_0^\infty F(n;E)\,\frac{\sigma_{\mathrm{capt}}(E)}{\sigma_{\mathrm{tot}}(E)}\,dE, \tag{10}$$

where $F(n;E)$ is the population distribution calculated for incident energy E, σ_{capt} is the capture cross section, σ_{tot} is the total ionization cross section, and N is a normalization constant such that

$$\sum_{n=1}^{\infty} P(n)=1.$$

Under the same assumption, the probability of capture by component i in a binary mixture is given by

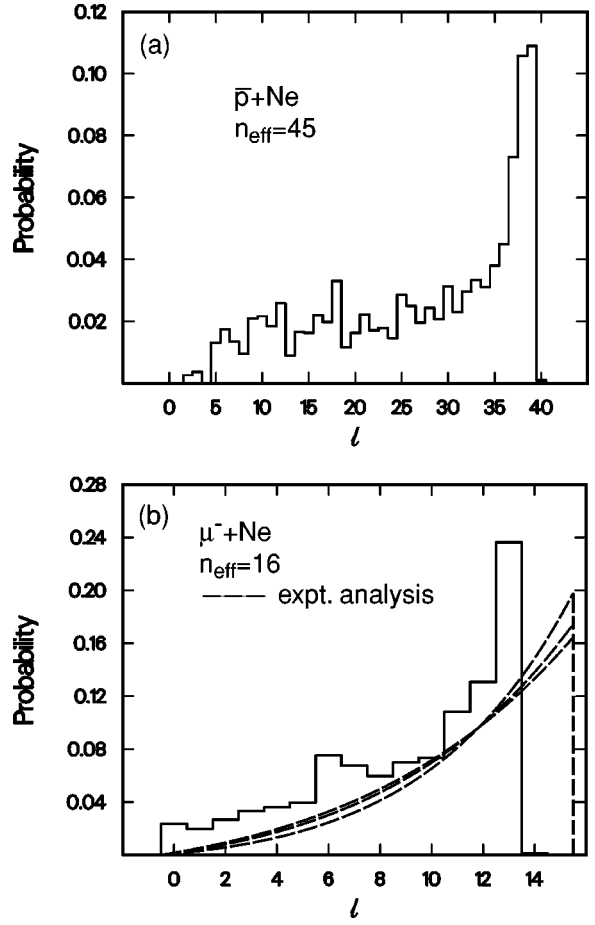

FIG. 11. Angular-momentum l distributions for (a) $\bar{p}$ captured by neon in $n_{\mathrm{eff}}=45$ and (b) μ^- captured by neon in $n_{\mathrm{eff}}=16$. This analysis was done with the n quantum number defined by Eq. (9). Note that, in this effective-charge analysis, $l_{\max}<n-1$ (see text). The dashed curves in (b) are the experimental fits (Ref. [18]) obtained assuming the form $(2l+1)e^{\alpha l}$ with $\alpha=0.090$ (central value) and 0.075 and 0.125 (error limits).

$$W_i \approx N \int_0^{\infty} \frac{c_i \sigma_{\mathrm{capt}}^{(i)}(E_{\mathrm{lab}})}{c_1 \sigma_{\mathrm{tot}}^{(1)}(E_{\mathrm{lab}}) + c_2 \sigma_{\mathrm{tot}}^{(2)}(E_{\mathrm{lab}})} dE_{\mathrm{lab}}, \qquad (11)$$

where c_1 and c_2 are the atomic concentrations of each species (here He and Ne), $c_1+c_2=1$, and N is a normalization constant such that $P_{\mathrm{capt}}^{(1)}+P_{\mathrm{capt}}^{(2)}=1$. The cross sections in this expression are those shown in Fig. 4(a) for $\bar{p}$+He/Ne and Fig. 4(b) for μ^-+He/Ne, transformed to the laboratory system using

$$E_{\mathrm{lab}} = \left(1 + \frac{m_x}{m_t}\right) E_{\mathrm{c.m.}}, \qquad (12)$$

where m_t is the target mass and m_x is the projectile ($\bar{p}$ or μ^-) mass. Except for $\bar{p}$+He, the differences of the plots as a function of $E_{\mathrm{c.m.}}$ and E_{lab} would barely be noticeable on the scale of this figure.

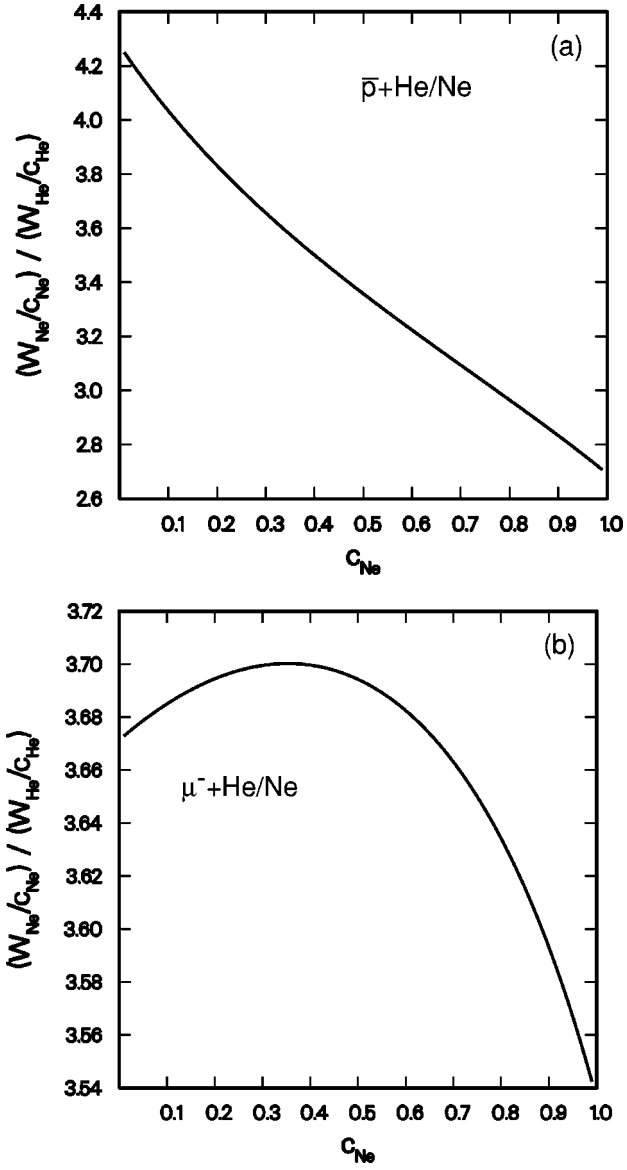

FIG. 12. Reduced capture ratios for (a) $\bar{p}$ and (b) μ^- captured in mixtures of helium and neon.

The most informative way of looking at capture is the reduced capture ratio, i.e., the ratio of capture probabilities *per atom*

$$A(Z_1,Z_2) = \frac{W(Z_1)/c(Z_1)}{W(Z_2)/c(Z_2)}. \qquad (13)$$

If the process is linear in Z then this ratio is independent of c_{Ne}; however, as first pointed out by Vogel *et al.* [50], this ratio can in fact depend on the concentration. The reduced capture ratios for $\bar{p}$ and μ^- in Ne:He mixtures are shown in Figs. 12(a) and 12(b), respectively. In both cases the probability of capture by neon is the greater, as expected from its capture cross sections reaching much higher energies. For a 50:50 mixture, the reduced ratios are similar, $A(\mathrm{Ne,He})=3.36$ for $\bar{p}$ and $A(\mathrm{Ne,He})=3.69$ for μ^-.

TABLE IV. Reduced capture ratios and average capture energies for (a) $\bar{p}$ and (b) μ^- in neon-helium mixtures.

C(Ne)	A(Ne,He)	$\bar{E}^{\rm lab}_{\rm capt}$ (eV)		
		He	Ne	Average
		(a) $\bar{p}$ capture		
0.01	4.25	21.4	70.1	21.9
0.10	4.04	20.5	67.6	26.5
0.50	3.36	17.6	59.5	40.7
0.90	2.83	14.0	53.2	50.2
0.99	2.71	12.9	51.8	51.6
		(b) μ^- capture		
0.01	3.67	21.1	63.0	21.6
0.10	3.69	20.8	64.1	26.3
0.50	3.69	18.9	68.2	50.5
0.90	3.59	16.2	71.4	68.4
0.99	3.54	15.4	72.2	72.0

Upon closer inspection, there is a significant difference between the dependencies on the mixture fractions in the two cases. The reduced capture ratio for $\bar{p}$, shown in Fig. 12(a), has a substantial monotonic dependence on the mixture, varying from 4.3 in predominantly helium to 2.7 in predominantly neon. This variation is due to the total ionization cross section for $\bar{p}$ collisions with neon being about twice as large as the total ionization cross section for $\bar{p}$ collisions with helium, as shown in Fig. 4(a). Thus an increased neon fraction increases the effective slowing-down cross section [in the denominator of Eq. (11)] and enables more $\bar{p}$ to reach the lower energies where capture by helium becomes possible, as indicated in Table IV. On the other hand, the reduced capture ratio for μ^-, shown in Fig. 12(b), is much less dependent on the mixture. This behavior is like that previously found for capture in mixtures of hydrogen and deuterium [51]. The dependence is weak because the total ionization cross sections for μ^-+He and μ^-+Ne are similar; thus their weighted sum in the denominator of Eq. (11) is almost constant. The slight maximum at $c_{\rm Ne}\approx 0.35$ is due to the crossing of the μ^-+He and μ^-+Ne total ionization cross sections at ~ 8 a.u.

There have been a number of experimental determinations of capture ratios for helium and neon using negative muons and pions. (The π^- mass is close enough to that of the μ^- that the atomic capture properties can be expected to be about the same.) All of the capture ratios between ^{4}He and

TABLE V. Comparison with experimental capture ratios. Uncertainties do not include errors due to the intermediary gas for indirectly determined ratios.

$A(Z_1,Z_2)$	Projectile	Target (Z_1:Z_2)	Intermediary gas	Source
3.5−3.7[a]	μ^-	Ne:^{4}He	none	Present calculation
3.4±0.7	μ^-	Ne:^{4}He	Ar	Hutson *et al.*[b]
4.1±0.3	μ^-	Ne:^{4}He	Ar	Budyashov *et al.*[c]
4.2±0.3	π^-	Ne:^{4}He	H_2	Petrukhin *et al.*[d]
5.5±1.0	π^-	Ne:^{4}He	^{3}He	Bannikov *et al.*[e]
3.5−3.7	μ^-	Ne:^{3}He	none	Present calculation
4.13±0.15	π^-	Ne:^{3}He	none	Bannikov *et al.*[e]
0.99	μ^-	^{4}He:^{3}He	none	Present calculation
0.75±0.13	π^-	^{4}He:^{3}He	none	Bannikov *et al.*[e]

[a]This is the range for different neon concentrations.
[b]Reference [13].
[c]Reference [12].
[d]Reference [14].
[e]Reference [15].

Ne have been determined indirectly. The capture fraction of helium is measured with some third species (Ar, H_2, or ^{3}He) and the capture fraction of neon with that same species; then the ratio of these two measurements is assumed to give the ratio that would be obtained with a mixture of helium and neon. Though there is no rigorous theoretical basis for this assumption, there is empirical evidence for its validity in chemical compounds [52]. The results of these measurements are given in Table V. The experimental values bracket the presently calculated reduced capture ratio of ~ 3.6 shown in Fig. 12(b). It is not known to what extent the deviations may be due to the indirect method of determination.

The concentration dependence of the reduced capture ratios for neon and helium has not been measured experimentally. Measurements of the concentration dependence for μ^- capture in argon-neon, krypton-argon, and xenon-argon mixtures have been reported by Ehrhart *et al.* [53]. For the first two mixtures, they found a significant concentration dependence, about as strong as we calculate for $\bar{p}$ in the neon-helium mixture. However, it is in the oppposite direction; A(Ar,Ne) and A(Kr,Ar) *increase* as the fraction of the heavier element increases, while we find A(Ne,He) decreases as the neon fraction increases. Though we have no knowledge of the total cross sections for argon and krypton that controverts opposing behaviors, it may be noted that the absolute numbers of Ehrhart *et al.* [53] for A(Ar,Ne) and A(Kr,Ar) disagree with other experiments [12,13,54].

The experiment of Bannikov *et al.* [15] found the reduced capture ratio of pions in a ^{4}He:^{3}He mixture to be 0.75 ± 0.13. This result differs from unity by only 2 sigma, and they were careful not to claim *proof* of an isotope effect. An isotope effect of this magnitude would be quite surprising since the electronic structures are the same and the π^- is much lighter than either nucleus. Therefore we have done FMD calculations on $\mu^- + {}^3$He and $\bar{p} + {}^3$He for comparison with the similar calculations on ^{4}He targets reported in Sec. III. The cross sections for ^{3}He in its center-of-mass system were found to agree with those for ^{4}He within the Monte Carlo error bars in all cases. Using these cross sections, reduced capture ratios $A(^4\text{He},^3\text{He})$ were calculated as 0.991 for μ^- and 0.890 for $\bar{p}$ [the dependence on $c(^3\text{He})$ is extremely weak].

To see how much of this small isotope effect might be due to the center-of-mass cross sections and how much to their transformation to the laboratory system, we repeated the calculation using *exactly* the same center-of-mass cross sections. This result was negligibly different, 0.987 for μ^- and 0.900 for $\bar{p}$. The ratio for π^- should be close to that for μ^-; in any event, a ratio as small as 0.75 seems unlikely. If we compare with the value of 4.13 directly obtained experimentally with Ne:^{3}He mixtures, instead of with the indirect Ne:^{4}He value, the agreement with the present calculation and with other experiments is considerably improved.

VI. CONCLUSIONS

The present calculations have demonstrated key features of the negative-particle capture process. Our results for $\bar{p}$ and μ^- capture by helium and neon suggest that the capture probabilities of increasingly heavy atoms grow both because more electrons are ionized and because the additional electrons carry off larger kinetic energies. The oft-invoked quasiadiabatic arguments are still fairly descriptive of capture by helium, but are virtually useless for the ten-electron neon atom. For neon, multiple ionization occurs and the residual ion is generally left in a shake-up state. Comparison of our results with recent experiments on muonic neon [18] suggests that many of the attached electrons autoionize without changing the atomic state of the exotic particle. Only subsequently can electron emission be unambiguously associated with cascading transitions of the exotic particle. In the interim, the convenient assumption that Auger steps in the cascade occur with the electron making transitions between adiabatic ground states is not valid. Another experiment with antiprotonic neon [55] confirms that our neglect of x-ray emission during the initial Auger relaxation is valid and showed that the cascade in antiprotonic neon is nearly circular at least by $n=15$.

Really, the various ionization processes proceed continuously and the instant of capture is not sharply defined. For this reason, we chose to follow the trajectory until the exotic particle reached some specified principal quantum number, which can provide a reasonable starting point for a quantum-mechanical cascade calculation. We observed a propensity for the exotic particle to reach circular orbits ($l=n-1$) at moderate n. The angular-momentum distributions are considerably more peaked at $l=n-1$ than can be represented by the $(2l+1)e^{\alpha l}$ distribution often assumed. We also found that the interpretation of the exotic particle as in a hydrogenic orbital with a screened nuclear charge [56] can be misleading since it distorts the all-important population of the angular-momentum states near $n-1$.

Within the limitations of the model used in analyzing a recent experiment on negative muon capture by neon [18], we obtained satisfactory agreement with the inferred number of bound electrons and the angular-momentum distribution. Fairly good agreement was also obtained with a number of experiments determining relative capture in helium and neon mixtures. However, a strong isotope effect on the capture of pions in mixtures of ^{3}He and ^{4}He, as suggested by one of the experiments [15], is not consistent with our calculations.

All experiments to date have used thick targets. Future experiments with monoenergetic beams of very slow antiprotons passing through thin targets promise to shed more light on the capture dynamics [7]. Capture at a known collision energy would avoid the complication resulting from competition between the slowing down and capture processes. For antiprotons in a helium-neon mixture we predict that this competition causes the per-atom capture probabilities to vary significantly with neon fraction.

ACKNOWLEDGMENTS

I am grateful to F. J. Hartmann, D. Horváth, K. S. Kirch, F. Kottmann, and L. M. Simons for helpful comments. This work was performed under the auspices of the U.S. Department of Energy.

APPENDIX: PROOF THAT $l \leqslant n$ CLASSICALLY

The energy of a single negative charge bound by a positive charge $+Z$ can be written

$$E = -\frac{Z}{r} + \frac{p_r^2}{2\mu} + \frac{l^2}{2\mu r^2} \tag{A1}$$

in terms of the radial momentum p_r and angular momentum l. We define the pseudoquantum number n by

$$n^2 = -\frac{\mu Z^2}{2E}. \tag{A2}$$

Then

$$n^2 = \frac{-\mu^2 Z^2 r^2}{-2\mu Z r + p_r^2 r^2 + l^2}, \tag{A3}$$

or

$$l^2 = 2\mu ZR - p_r^2 r^2 - \frac{\mu^2 Z^2}{n^2} r^2. \tag{A4}$$

It follows by maximization of l with respect to p_r and r that

$$l_{\max} = n \tag{A5}$$

is achieved when $p_r = 0$ and $r = n^2/\mu Z$.

In the present application, n is always large enough that the distortion of the Coulomb potential on the exotic particle by the nonclassical FMD pseudopotentials is negligible.

[1] W. Barkas, J. Dyer, and H. Heckman, Phys. Rev. Lett. **11**, 26 (1963).

[2] D. Horváth and R.M. Lambrecht, *Exotic Atoms, A Bibliography 1939–1982* (Elsevier, Amsterdam, 1984).

[3] E. Fermi and E. Teller, Phys. Rev. **72**, 399 (1947).

[4] V.G. Zinov, A.D. Konin, and A.I. Mukhin, Yad. Fiz. **2**, 859 (1965) [Sov. J. Nucl. Phys. **2**, 613 (1966)].

[5] J.S. Cohen, in *Electromagnetic Cascade and Chemistry of Exotic Atoms*, edited by L.M. Simons, D. Horváth, and G. Torelli (Plenum, New York, 1990), pp. 1–22.

[6] J.S. Cohen, J. Phys. B **31**, L833 (1998).

[7] ASACUSA collaboration proposal CERN/SPSC 97-19, SPSC P-307 (1997).

[8] A.S. Wightman, Phys. Rev. **77**, 521 (1950).

[9] H. Schneuwly, V.I. Pokrovsky, and V.I. Ponomarev, Nucl. Phys. A **312**, 419 (1978).

[10] H. Daniel, Z. Phys. A **291**, 29 (1979).

[11] T. von Egidy, D.H. Jakubassa-Amundsen, and F.J. Hartmann, Phys. Rev. A **29**, 455 (1984).

[12] Yu.G. Budyashov, V.G. Zinov, A.D. Konin, and A.I. Mukhin, Yad. Fiz. **5**, 830 (1967) [Sov. J. Nucl. Phys. **5**, 589 (1967)].

[13] R.L. Hutson, J.D. Knight, M. Leon, M.E. Schillaci, H.B. Knowles, and J.J. Reidy, Phys. Lett. A **76**, 226 (1980).

[14] V.I. Petrukhin and V.M. Suvorov, Zh. Éksp. Teor. Fiz. **70**, 1145 (1976) [Sov. Phys. JETP **43**, 595 (1976)].

[15] A.V. Bannikov, B. Lévay, V.I. Petrukhin, V.A. Vasilyev, L.M. Kochenda, A.A. Markov, V.I. Medvedev, G.L. Sokolov, I.I. Strakovsky, and D. Horváth, Nucl. Phys. A **403**, 515 (1983).

[16] N.H. Kwong, J.D. Garcia, and J.S. Cohen, J. Phys. B **22**, L633 (1989).

[17] For a review, see L. Wilets and J.S. Cohen, Contemp. Phys. **39**, 163 (1998).

[18] K. Kirch, D. Abbott, B. Bach, P. Hauser, P. Indelicato, F. Kottmann, J. Missimer, P. Patte, R.T. Siegel, L.M. Simons, and D. Viel, Phys. Rev. A **59**, 3375 (1999).

[19] C.L. Kirschbaum and L. Wilets, Phys. Rev. A **21**, 834 (1980).

[20] J.S. Cohen, Phys. Rev. A **51**, 266 (1995); **57**, 4964 (1998).

[21] W.A. Beck and L. Wilets, Phys. Rev. A **55**, 2821 (1997).

[22] J.S. Cohen, Phys. Rev. A **54**, 573 (1996).

[23] F.J. Hartmann, in *Electromagnetic Cascade and Chemistry of Exotic Atoms* (Ref. [5]), pp. 127–139.

[24] R. Landua and E. Klempt, Phys. Rev. Lett. **48**, 1722 (1982).

[25] R.J. Wetmore, D.C. Buckle, J.R. Kane, and R.T. Siegel, Phys. Rev. Lett. **19**, 1003 (1967).

[26] A. Placci, E. Polacco, E. Zavattini, K. Ziock, G. Carboni, U. Gastaldi, G. Gorini, G. Neri, and G. Torelli, Nuovo Cimento A **1**, 445 (1971).

[27] G. Backenstoss, J. Egger, T. von Egidy, R. Hagelberg, C.J. Herrlander, H. Koch, H.P. Povel, A. Schwitter, and L. Tauscher, Nucl. Phys. A **232**, 519 (1974).

[28] H.P. von Arb, F. Dittus, H. Heeb, H. Hofer, F. Kottmann, S. Niggli, R. Schaeren, D. Taqqu, J. Unternährer, and P. Egelhof, Phys. Lett. B **136**, 232 (1984).

[29] M. Eckhause, P. Guss, D. Joyce, J.R. Kane, R.T. Siegel, W. Vulcan, R.E. Welsh, R. Whyley, R. Dietlicher, and A. Zehnder, Phys. Rev. A **33**, 1743 (1986).

[30] A. Blaer, J. French, A.M. Sachs, M. May, and E. Zavattini, Phys. Rev. A **40**, 158 (1989).

[31] S. Tresch, F. Mulhauser, C. Piller, L.A. Schaller, L. Schellenberg, H. Schneuwly, Y.A. Thalmann, A. Werthmüller, P. Ackerbauer, W.H. Breunlich, M. Cargnelli, B. Gartner, R. King, B. Lauss, J. Marton, W. Prymas, J. Zmeskal, C. Petitjean, M. Augsburger, D. Chatellard, J.P. Egger, E. Jeannet, T. von Egidy, F.J. Hartmann, M. Mühlbauer, and W. Schott, Phys. Rev. A **58**, 3528 (1998).

[32] R. Abela, G. Backenstoss, A.B. d'Oliveira, M. Izycki, H.O. Meyer, I. Schwanner, L. Tauscher, P. Blüm, W. Fetscher, D. Gotta, H. Koch, H. Poth, and L.M. Simons, Phys. Lett. B **68**, 429 (1977).

[33] C.J. Batty, S.F. Biagi, S.D. Hoath, P. Sharman, J.D. Davies, G.J. Pyle, and G.T.A. Squier, Nucl. Phys. A **326**, 455 (1979).

[34] J.D. Davies, T.P. Gorringe, J. Lowe, J.M. Nelson, S.M. Playfer, G.J. Pyle, G.T.A. Squier, C.A. Baker, C.J. Batty, S.A. Clark, S. Sakamoto, R.E. Welsh, R.G. Winter, and E.W.A.

Lingeman, Phys. Lett. B **145**, 319 (1984).
[35] C.A. Baker, C.J. Batty, J. Moir, S. Sakamoto, J.D. Davies, J. Lowe, J.M. Nelson, G.J. Pyle, G.T.A. Squier, R.E. Welsh, R.G. Winter, and E.W.A. Lingeman, Nucl. Phys. A **494**, 507 (1989).
[36] M. Schneider, R. Bacher, P. Blüm, D. Gotta, K. Heitlinger, W. Kunold, D. Rohmann, J. Egger, L.M. Simons, and K. Elsener, Z. Phys. A **338**, 217 (1991).
[37] M. Iwasaki, S.N. Nakamura, K. Shigaki, Y. Shimizu, H. Tamura, T. Ishikawa, R.S. Hayano, E. Takada, E. Widmann, H. Outa, M. Aoki, P. Kitching, and T. Yamazaki, Phys. Rev. Lett. **67**, 1246 (1991).
[38] E. Widmann, I. Sugai, T. Yamazaki, R.S. Hayano, M. Iwasaki, S.N. Nakamura, H. Tamura, T.M. Ito, A. Kawachi, N. Nishida, W. Higemoto, Y. Ito, N. Morita, F.J. Hartmann, H. Daniel, T. von Egidy, W. Schmid, J. Hoffmann, and J. Eades, Phys. Rev. A **51**, 2870 (1995).
[39] R.S. Hayano, T. Ishikawa, H. Tamura, H.A. Torii, M. Hori, F.E. Maas, N. Morita, M. Kumakura, I. Sugai, F.J. Hartmann, H. Daniel, T. von Egidy, B. Ketzer, R. Pohl, D. Horváth, J. Eades, E. Widmann, and T. Yamazaki, Phys. Rev. A **55**, R1 (1997).
[40] B. Ketzer, F.J. Hartmann, T. von Egidy, C. Maierl, R. Pohl, J. Eades, E. Widmann, T. Yamazaki, M. Kumakura, N. Morita, R.S. Hayano, M. Hori, T. Ishikawa, H.A. Torii, I. Sugai, and D. Horváth, Phys. Rev. Lett. **78**, 1671 (1997).
[41] G.Ya. Korenman and S.I. Rogovaya, Radiat. Eff. **46**, 189 (1980).
[42] P.K. Haff and T.A. Tombrello, Ann. Phys. (N.Y.) **86**, 178 (1974).
[43] N.A. Cherepkov and L.V. Chernysheva, Yad. Fiz. **32**, 709 (1980) [Sov. J. Nucl. Phys. **32**, 366 (1980)].
[44] J.S. Cohen, R.L. Martin, and W.R. Wadt, Phys. Rev. A **27**, 1821 (1983).
[45] V.K. Dolinov, G.Ya. Korenman, I.V. Moskalenko, and V.P. Popov, Muon Catal. Fusion **4**, 169 (1989).
[46] G.Ya. Korenman, Hyperfine Interact. **101/102**, 81 (1996).
[47] W.A. Beck, L. Wilets, and M.A. Alberg, Phys. Rev. A **48**, 2779 (1993).
[48] M. Leon, Phys. Rev. A **17**, 2112 (1978).
[49] J.S. Cohen, R.L. Martin, and W.R. Wadt, Phys. Rev. A **24**, 33 (1981).
[50] P. Vogel, P.K. Haff, V. Akylas, and A. Winther, Nucl. Phys. A **254**, 445 (1975).
[51] J.S. Cohen, Phys. Rev. A **59**, 1160 (1999).
[52] T. von Egidy and F.J. Hartmann, Phys. Rev. A **26**, 2355 (1982).
[53] P. Ehrhart, F.J. Hartmann, E. Köhler, and H. Daniel, Phys. Rev. A **27**, 575 (1983); Z. Phys. A **311**, 259 (1983).
[54] H.-J. Pfeiffer, K. Springer, and H. Daniel, Nucl. Phys. A **254**, 433 (1975).
[55] R. Bacher, P. Blüm, D. Gotta, K. Heitlinger, M. Schneider, J. Missimer, L.M. Simons, and K. Elsener, Phys. Rev. A **38**, 4395 (1988).
[56] J.E. Griffith, P.K. Haff, and T.A. Tombrello, Ann. Phys. (N.Y.) **87**, 1 (1974).